Inorganic Chemistry Research

Article

Mononuclear Nickel(II) and Zinc(II) Complexes with N-(2-propanamide)-2-picolylamine Ligand: Synthesis, Chromotropism Properties and DFT Calculations

Marzieh Asadollahi, Hamid Golchoubian* and Atie Shirvan*

Department of Chemistry, University of Mazandaran, Babol-sar 47416-95447, Iran

Received: March 11, 2023; Accepted: May 3, 2023

Cite This: *Inorg. Chem. Res.* **2022**, *6*, 146-154. DOI: 10.22036/icr.2023.389361.1142

Abstract: Two nickel(II), and zinc(II) complexes $[ML_2](ClO_4)_2$ of N-(2-propanamide)-2-picolylamine, L, derived from the condensation reaction of 2-picolylamine with acrylamide were synthesized. The prepared complexes were characterized by elemental analyses, ultraviolet-visible, infrared, 1-H-NMR spectroscopy techniques, and conductivity measurements. The ligand behaves like an NNO donor set, forming octahedral geometries with both Ni(II) and Zn(II) complexes. The nickel complex is halochromic. pH effects on the visible absorption spectra of the nickel complex were investigated in the range of 2-13. Its color change was due to the protonation and deprotonation of labile moieties of the ligand at room temperature. The complex displayed reversible thermochromism in solvents of DMSO and DMF attributed to the dissociation of hemilabile amide moieties from the metal center and substituted by solvent molecules. For the purpose of assigning experimental data to the ligands and complexes, a density function theory calculation on the level of B3LYP/LanL2DZ was performed.

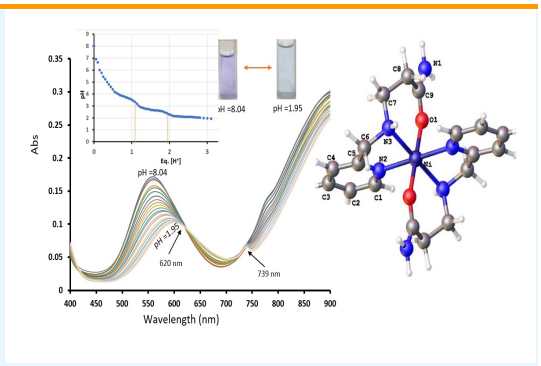

Keywords: 2-Picolylamine derivative, Nickel complex, Zinc complex, Chromotropism, DFT

1. INTRODUCTION

Research is currently focused on the synthesis of chelated ligands containing mixed functionalities attached to transition metal centers. In particular, the chemistry of hemilabile ligands is of special interest.[1-9] The molecules containing different functional groups, such as soft donor and hard donor, are considered hemilabile ligands and are used increasingly in a variety of molecular chemistry applications, including molecular activation, homogeneous catalysis, functional materials, and small-molecule sensing.[2,8-10] The ability of hemilabile coordination complexes to reversibly bond to metal centers has recently led to their use as small molecule chemosensors.[11] Multifunctional ligands that contain amide moieties are therefore qualified candidates for showing hemilability. An example of such a hemilabile ligand is an amide–amine compound.[12-14] A substantially inert amine group along with a labile amide group makes this category of ligands hemilabile. In addition, there are two types of coordination modes for the amide group, O-bound, where the metallation process takes place via carbonyl oxygen and amidated complexes that bond through the nitrogen atom in an alkaline environment. It is possible to prepare chromotropic materials by coordinating these ligands with suitable metal ions. Because nickel(II) has different coordination numbers and geometric structures, it is a good candidate for d-d transitions that lead to color changes.[15,16] In chromotropism, changes in optical properties (transparency or light diffraction) occur that are caused by changes in the structure of compounds that occur upon stimulation of the chemical or physical environment such as solvents (solvatochromism), temperatures (thermochromisms), pressures (pizochroms), light (photochromisms), pH (halochromisms), ions (ionochromisms), etc. Our interest in chromotropic metal complexes involving 2-picolylamine-derived ligands has been further advanced[17,18] by preparing two new Ni(II) and Zn(II) complexes containing N-(2-propanamide)-2-picolylamine as a ligand (L) shown in Scheme 1, which is obtained by condensation of 2-picolylamine with acrylamide.

2. EXPERIMENTAL

Materials and methods

The ligand was prepared as described in our published

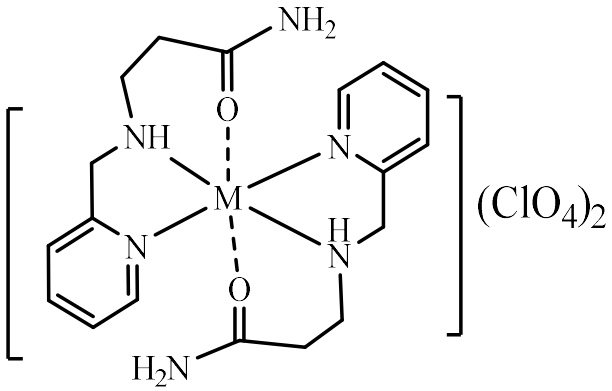

M= Ni, **1** and Zn, **2**

Scheme 1. The structure of the complexes under study

procedures.[12] The chemicals used were all commercially available (reagent grade). Elemental analyses for C, H, and N were performed on a Perkin Elmer Model 2400 elemental analyzer. A Jenway 400 conductance meter was used to measure conductivities in methanol, water, and dimethylformamide solution at 25°C. A Bruker FT-IR spectrophotometer was used to record IR spectra of KBr pellets in the region of 4000–600 cm^{-1}. A Jasco V-530 UV-Vis spectrophotometer with quartz cells of 1 cm was used to measure the electronic absorption spectra in the 200-800 nm range. A Bruker 400DRX spectrometer was used to record 1-H NMR spectra with tetramethylsilane as the internal standard. Chemical shifts (δ) are expressed in ppm.

Preparation of the complexes

$[NiL_2](ClO_4)_2$, 1. A solution of $Ni(ClO_4)_2 \cdot 6H_2O$ (0.73 g, 2 mmol) in methanol (10 ml) was added to a solution of ligand (0.71 g, 4 mmol) in methanol (12 ml). The reaction mixture was stirred at room temperature for 3 hours. The purple precipitate was separated by filtration and dried under a vacuum. The crude product was recrystallized by diffusion of diethyl ether into an acetonitrile solution. Yielded pale purple crystals (0.44 grams, 36%). Anal. Calcd. for $C_{18}H_{26}Cl_2NiN_6O_{10}$ (MW = 616.03 g mol^{-1}): C, 35.10; H, 4.25; N, 13.64; found C, 34.74; H, 4.08; N, 13.36. Selected IR data ($\bar{\upsilon}$/cm^{-1}using KBr disk): 3463 and 3361 (m, doublet, NH_2 str.), 3291 (m, N-H str.), 3093 (w, C-H aromatic.), 2926 (w, C-H aliphatic.), 1657 (s, C=O str.), 1609 (m, N-H bend.), 1605 (s, C-N str.), 1084 (s, ClO_4 str.).

$[ZnL_2](ClO_4)_2$, 2. A similar reaction procedure as described for complex **1** was followed except $Zn(ClO_4)_2 \cdot 6H_2O$ was used instead of $Ni(ClO_4)_2 \cdot 6H_2O$. Yielded 0.28 g, 46% as colorless crystals. Anal. Calcd. for $C_{18}H_{26}Cl_2ZnN_6O_{10}$ (MW = 620.04 g mol^{-1}): C, 34.72; H, 4.21; N, 13.50; found C, 34.64; H, 4.11; N, 13.40. Selected IR data ($\bar{\upsilon}$/cm^{-1}using KBr disk): 3438 and 3353 (m, doublet, NH_2 str.), 3291 (m, N-H str.), 3109 (w, C-H aromatic.), 2948 (w, C-H aliphatic.), 1661 (s, C=O str.), 1609 (m, N-H bend.), 1604 (s, C-N str.), 1087 (s, ClO_4 str.). ^{1}H-NMR (400 MHz, MeOD), **δ:** 2.61 (M, 2H, **-CH_2**$CH_2C(O)NH_2$); 3.45 (M, 2H, **-CH_2**$C(O)NH_2$); 2.64 (s, 2H, **-CH_2**-Py); 7.54 (M, 4H, Py); 8.18 (M, 4H, Py).

Computational details

A Gaussian09 program[19] was used for all calculations. The output files were visualized using GaussView 05 software.[20] Based on the B3LYP/LanL2DZ level of theory, geometry optimization was carried out with +2 charge for the complexes and zero charges for the ligand, as well as triplet spin multiplicities for $[NiL_2]^{2+}$ and singlet spin multiplicities for $[ZnL_2]^{2+}$,[21]. A molecular system containing transition metals can be provided with good geometries by choosing this function.[22] According to the calculated vibrational spectra, the minima on the potential energy surfaces are devoid of negative imaginary frequencies, which corresponding to the true minimum energy. A Gaussian program was used to calculate the atom movements in Cartesian coordinates in order to assign approximate frequencies to molecular vibrational modes. GaussView was used to animate each molecular vibrational mode based on the calculated atom movements. In terms of electrical and optical properties, as well as chemical reactions, frontier molecular orbitals play a key role in molecular dynamics.[24] Molecular chemical stability is characterized by the gap between HOMO and LUMO.[25] As a result of employing Koopmans's theorem,[26] the energy of frontier molecular orbitals is determined by the ionization energy (IE) and electron affinity (EA) of the present compounds. The absolute electronegativity (χ), chemical potential (μ), and softness (σ) indices have been derived by computing the gaps between HOMO and LUMO levels and the Mulliken atomic charge distribution.[27] In addition to the dipole moment, there are several other properties of interest that can be calculated based on the energy gap between HOMO and LUMO levels.[28,29] calculated as follows: *I*: ionization potential = E_{HOMO}, *A*: electron affinity = E_{LUMO}, ΔE_{gap}: the energy gap (eV) = E_{LUMO} -E_{HOMO}, Electronegativity (χ) = $(I + A)/2$, Hardness (η) = $(I - A)/2$, Softness (σ) = 1/η, Chemical potential (μ) = -χ, Electrophilicity (ω) = $\mu^2/2\eta$

3. RESULTS AND DISCUSSION

Synthesis

The complexes were obtained by reacting the ligand with metal(II) perchlorate at room temperature. The visible spectral titration experiment was used to determine binding stoichiometry in the complex. In order to accomplish this, an aqueous solution of $Ni(ClO_4)_2 \cdot 6H2O$ (3×10^{-5} mol/L) was added in different proportions to the ligand L solution (3×10^{-5} mol/L), and a change in visible spectra of the solution was examined. As it is shown in Fig. 1, titration curves reveal significant changes in the absorption bands of ligand L. As Ni^{2+} ion concentrations are increased, the absorption bands at about 560 nm and 900 nm gradually increase. The endpoint of the titration is reached when the molar ratio of the ligand L to Ni^{2+} ion is 2:1 (see inside Fig. 1). It is noteworthy that the reaction of copper(II) perchlorate with the same ligand resulted in the formation of $[CuL(H_2O)_2](ClO_4)_2$ and $[CuL_2](ClO_4)_2$ after the addition of one and two molar equivalents of the ligand to copper(II), respectively. Both compounds (as illustrated in scheme 1) are stable in air at room temperature, soluble in DMF, DMSO, MeOH, EtOH, MeCN, and water, and poorly soluble in low polar solvents.

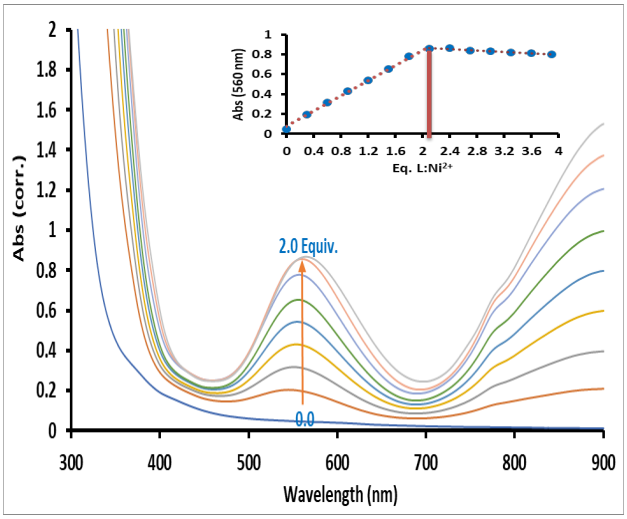

Fig. 1. Visible spectra of L with increasing concentrations of $Ni(ClO_4)_2{\cdot}6H_2O$. Inside figure molar ratio method: plots of Ni(II) with ligand measured at 560 nm of absorbance.

Characterization

IR spectra. Detailed experimental assignments of the vibrational bands of complexes are provided in Supporting Information Tables S1 and S2. A confirmation of the formation of metal(II) complexes can be obtained by means of IR spectroscopy. There was a strong absorption band in the IR spectrum of the ligand at 1667 cm^{-1}, which corresponds to $\nu_{C=O}$(amide) vibration shifting to lower energy in both complexes (1657 cm^{-1} and 1661 cm^{-1} in **1** and **2**, respectively) associated with the coordination of the amide moiety of the ligand and signifies that this group participates in the coordination via C=O. Due to the formation of C=O–M bonds, a redshift of ν(C=O) by 10-6 cm^{-1} is evident due to the participation of (C=O) group in the formation of complexes. In spite of this, the low redshifts of this complex in comparison to its analogous Cu(II) complex ($\Delta\nu$ = 12 cm^{-1}) [12] indicate that the M-O=C bond in both complexes is weak. In both complexes, an NH stretching vibration of the amine group appears as a narrow band with medium intensity. In contrast, the free ligand showed a wider band at a higher frequency.[30] The vibrational bands in the 3300-3450 cm^{-1} correspond to the stretching of NH_2 of the amide group, which appear almost at the same location as the free ligand. Furthermore, the stretching frequencies observed around 1609 cm^{-1} may be attributed to the bending vibration of NH_2. The perchlorate group exists as an anionic group in both complexes, as evidenced by a strong intensity band at 1089 in **1** and 1087 in **2**.[31]

Molar conductivity. In a solution of methanol, water, and dimethylformamide, the molar conductivity of the complexes was determined at 25 °C. The concentrations of the samples were 10.0×10^{-4}, 6.00×10^{-4}, 4.00×10^{-4} and 2.00×10^{-4} M. The molar conductances of each sample were then plotted against the concentrations of each solvent. A molar conductance value was obtained by extrapolating the curve to an infinitely diluted solution. Table 1 presents these values. The standard value of 1:2 electrolytes in various solvents is provided in this table.[32] Based on the conductivity data, it was found that both complexes contained 1:2 electrolytes.

Table 1. Molar conductance values (Λ_m) of the compounds (Ω^{-1} cm^2 mol^{-1}) at 25 °C in different solvents

Complexes	MeOH	H_2O	DMF
1	212	230	163
2	165	263	161
1:2 electrolytes	160-220	235-273	130-170

Electronic absorption spectra. The electronic spectrum of complex **1** in ab aqueous solution is shown in Fig. 2. Four spin-allowed transitions are expected to arise from ground term $^3A_{2g}$ under ideal conditions for a tetragonal distortion of the octahedral system (D_{4h}). In the visible region, $[NiL_2](ClO_4)_2$ shows two bands one above 900 nm ($\varepsilon \approx 15$ dm^3 mol^{-1} cm^{-1}) and another at 558 (ε = 9 dm^3 mol^{-1} cm^{-1}) nm as well as a shoulder at 770 nm ($\varepsilon \approx$ 7 dm^3 mol^{-1} cm^{-1}). Both of these bands occur as a result of transitions from $^3A_{2g}$ → $^3T_{2g}$ and $^3A_{2g}$ → $^3T_{1g}(^3F)$ (presuming the *N* and *O* site symmetry). The fourth band at higher energy is completely obscured by metal–ligand charge-transfer. These observations are consistent with a pseudo-octahedral geometry around Ni^{2+} ions and in agreement with NiN_4O_2 chromophores.[33,34] The bands situated at 259 nm (ε = 10420 dm^3 mol^{-1} cm^{-1}) and 203 nm (ε = 31370 dm^3 mol^{-1} cm^{-1}) are related to the pyridine to Ni(II) (LMCT) and inter ligand charge transfer (ILCT), respectively.[35]

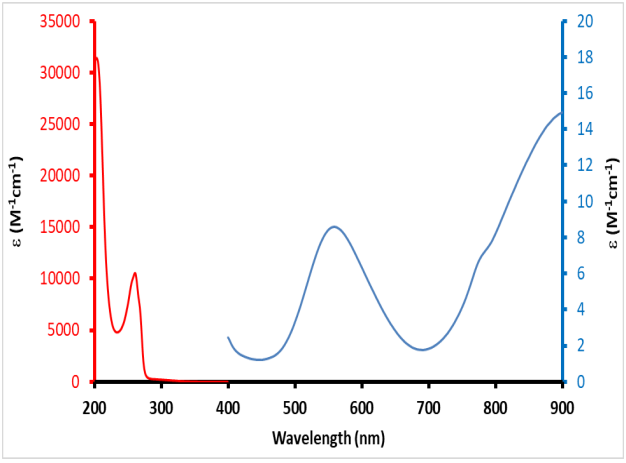

Fig. 2. UV-Vis absorption spectra of **1** in an aqueous solution. Charge transfer is presented on the left-side axis and d–d transition is displayed on the right-side axis.

Computational study. Density functional theory was used to optimize the structure of compounds in the

gaseous phase using the B3LYP/LanL2DZ level on the Gaussian 9. The calculated structural parameters are listed in Table 2. The contour shape of the optimized structure is shown in Fig. 2.

Table 2. Selected computed bond lengths (Å) and angles (°) for complexes

Bond lengths (Å)		
	$[NiL_2]^{2+}$	$[ZnL_2]^{2+}$
M(1)-N(2)	2.121	2.207
M(1)-O(1)	2.101	2.145
M(1)-N(3)	2.154	2.232
O(1)-C(9)	1.279	1.279
N(1)-C(9)	1.352	1.351
Bond angles (°)		
N(2)-M(1)-O(1)	89.247	87.808
N(2)-M(1)-N(3)	79.289	77.483
N(3)-M(1)- O(1)	88.232	89.589
N(3)-M(1)-N(2)#1	79.289	77.483
O(1)-M(1)-O(1)#1	179.999	179.989
N(3)-M(1)-N(3)#1	179.999	179.987
N(2)-M(1)-N(2)#1	179.999	179.959
N(1)-C(9)-O(1)	120.485	120.735

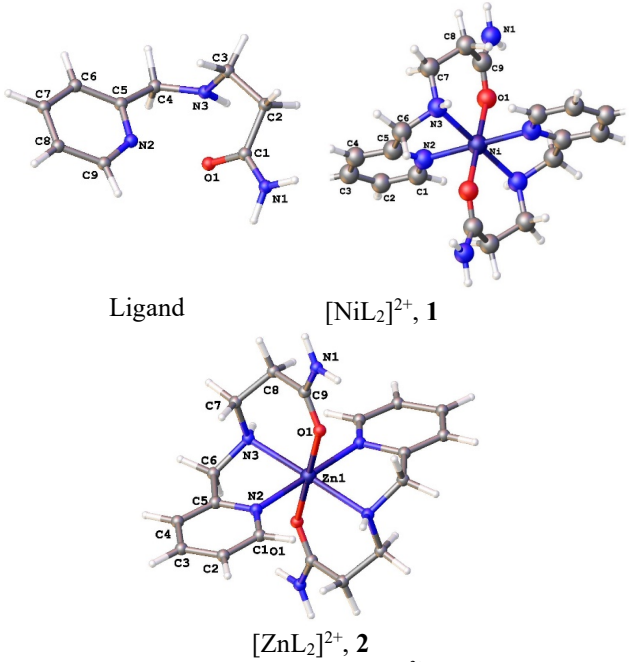

Fig. 2. Molecular modeling of ligand and $[ML_2]^{2+}$, the perchlorate anions was not shown.

The energy orbital diagrams of the HOMO (highest occupied molecular orbital) and LUMO (lowest unoccupied molecular orbital) of ligand L and complexes **1** and **2** are shown in Fig. 3. For the ligand L, the HOMO electron cloud is predominantly located on N-ethyl-2-ethylamide moiety whereas, the LUMO electron cloud is basically distributed on the pyridine rings. In $[NiL_2]^{2+}$, **1**, the electron clouds of HOMO are spread over the entire molecule (Ni: 22%, Pyridyl: 25%, amide chain: 53%) but the electron clouds of LUMO are distributed on the pyridine rings (Ni: 1%, Pyridyl: 98%, amide chain: 1%). The electron clouds of the HOMO in $[ZnL_2]^{2+}$, **2**, are distributed on Zn and the ligand (Zn: 3%, Pyridyl: 73%, amide chain: 24%) but in the LUMO the electron clouds distributed is almost the same as complex **1** and mainly distributed on the pyridine rings (Zn: 1%, Pyridyl: 99%, amide chain: 0%). In both complexes, compared with the ligand L, the electron cloud distribution is relatively concentrated. The energy gap of complexes **1** (ΔE = 4.9865 eV, or 249 nm) is smaller than **2** (ΔE = 5.7853 eV) which reveals the most reactive than complex **2** and with a higher value of softness (0.4011 eV). Charge transfer within the molecule can be facilitated by this process. Hence, the matching between the wavelength calculated for HOMO → LUMO (249 nm) with the experimental value of 259 nm arose from the amine chain and Ni(II) to the vacant orbitals (π*) of pyridine rings.

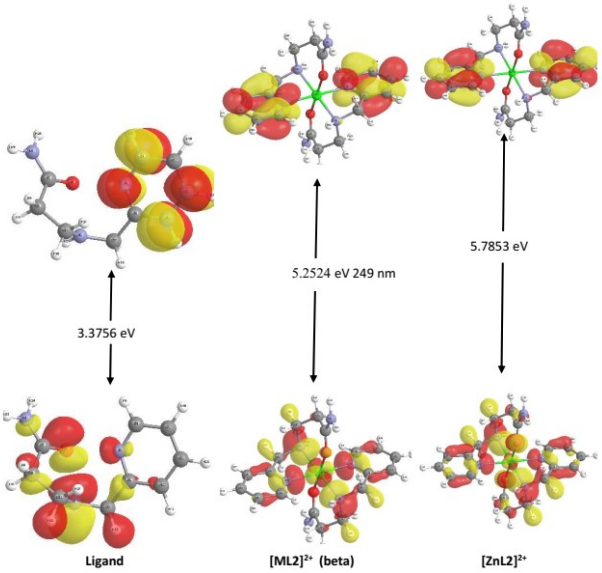

Fig. 3. HOMO and LUMO energy levels and energy gap diagrams of the ligand L, complexes **1** and **2**.

To gain a deeper understanding of chemical properties, density functional theory (DFT) was applied. The energy of HOMO indicates that the molecule is capable of donating electrons, while that of LUMO shows that it is capable of accepting electrons. A measure of reactivity known as global electrophilicity (ω/eV) is useful for comparing molecules in terms of their ability to donate electrons.[36] A strong nucleophile has a low electrophilicity value.[37] Therefore, as expected the ligand is a strong nucleophile. As shown in Table 3, both complexes are electrophile due to their cationic forms. However, a comparison between the two complexes shows that $[ZnL_2]^{2+}$ is the stronger electrophile. The dipole moment (D) of the ligand is 3.1761 Deby but this value for the complexes is negligible due to having the center of symmetric. The value of the chemical potential

(μ) revealed the stability and non-spontaneous decomposition of the complex molecule. All compounds show negative chemical potential and stability.

Table 3. Calculated chemical parameters of the ligand L and complexes **1** and **2** using B3LYP/LanL2DZ level of theory

	Ligand	$[NiL_2]^{2+}$	$[ZnL_2]^{2+}$
E_T (au)	-589.483482	-1349.370122	-1245.860047
E_{HOMO} (eV)	-3.6322	-6.7648	-7.5070
E_{LUMO} (eV)	-0.2566	-1.7783	-1.7217
E_{gap} (eV)	3.3756	4.9865	5.7853
I (eV)	3.6322	6.7648	7.5070
A (eV)	0.2566	1.7783	1.7217
χ (eV)	1.9444	4.2716	4.6144
Hardness η (eV)	1.6878	2.4933	2.8927
Softness σ (eV)	0.5925	0.4011	0.3457
Chemical potential μ (eV)	-1.9444	-4.2716	-4.6144
Electrophilicity ω (eV)	1.1200	3.6591	3.6804
D, Debye	3.1761	0.0010	0.0098

Despite the fact that the metal ions found in Table 4 are formally in the second oxidation state, the computed Mulliken charges were +0.361 in **1** and +1.034 in **2**, which are significantly lower than +2, which indicates that most of the electrons are retained from the ligand. It is therefore advantageous in these complexes to donate electrons from ligands to metals rather than back-donations from metals to ligands. Charge transfers between ligands and metal centers are confirmed by changes in atomic charges on donor ligands upon coordination. Due to back bonding from metal ions, the magnitude of the negative charge on N2 (-0.093), N3 (-0339), and O1 (-0389) increases slightly in both complexes (ranges from -0.181 to -0.418). However, the magnitude of the N1 atom of the amide group that is free from coordination compared with the free ligand L (amide nitrogen (-0.620)) is almost unchanged (-0.606 for **1** and -0.599 for **2**). It can be concluded that electron donation from the amide group to the metal may occur via its oxygen atom (O1), and the nitrogen atom (N1) of the amide group is uncoordinated. Metal(II) ions have 4s, 3d, and 4p orbitals in their natural electron configurations. Additionally, oxygen atoms as well as N(2) and N(3) atoms of the ligand with 2s and 2p orbitals share the same electron configuration and have small 3p contributions in both complexes.

FTIR spectroscopy. The calculated spectra of the compounds obtained by the DFT method at the B3LYP/LanL2DZ level are shown in Figs. 4, S1 and S2. In the experimental section, the prominent IR bands of ligands and complexes are assigned in 600 and 4000 cm^{-1}. For more investigation, selected experimental and calculated vibrational frequencies of the ligand and complexes are compared in Tables S1-S3. Both compounds exhibit almost identical FTIR spectra, which are in agreement with the molecular structures calculated for them. An analysis of the theoretical study elucidates and justifies the experimental results. On the basis of the

Table 4. NPA charges and natural electron configuration of ligand, nickel(II) and zinc(II) complexes using B3LYP/LanL2DZ level of theory in aqueous solvated

Complex	Atom	Charge[a]	Electron configuration
Ligand	N(1)	-0.620	[core]2S(0.69)2p(2.18)3p(0.01)
	N(2)	-0.093	[core]2S(0.70)2p(2.06)3p(0.01)
	N(3)	-0339	[core]2S(0.68)2p(2.14)3p(0.01)
	O(1)	-0.389	[core]2S(0.87)2p(2.49)3p(0.01)
$[NiL_2]^{2+}$	M(1)	+0.361	[core]4S(0.12)3d(3.37)4p(0.15)5p(0.07)
	N(1)	-0.606	[core]2S(0.67)2p(2.22)3p(0.01)
	N(2)	-0.181	[core]2S(0.67)2p(2.07)3p(0.01)
	N(3)	-0.421	[core]2S(0.68)2p(2.14)3p(0.01)
	O(1)	-0.347	[core]2S(0.84)2p(2.48)3p(0.01)
$[ZnL_2]^{2+}$	Zn(1)	+1.034	[core]4S(0.13)3d(4.99)4p(0.16)
	N(1)	-0.599	[core]2S(0.67)2p(2.22)3p(0.01)
	N(2)	-0.502	[core]2S(0.69)2p(2.11)3p(0.01)
	N(3)	-0.401	[core]2S(0.70)2p(2.19)3p(0.01)
	O(1)	-0.428	[core]2S(0.85)2p(2.52)3p(0.01)

[a]Atomic charge in units of e.

largest displacement of the atoms, vibrational frequencies were assigned for different vibrational movements. As shown in the IR spectra, the sharp bands with moderate intensities intensity at 3570, 3436, and 3391 cm^{-1} in **1** and 3573, 3437, and 3343 cm^{-1} in **2** correspond to the stretching frequencies of NH_2 of amide and NH of 2-picolyl amine, respectively.[38] In the complexes, the most intense bands occur around 1630 cm-1, corresponding to the bending of the C=O stretching of the amide groups, while these bands appear in the experimental spectra at approximately 1660 cm^{-1}. In the real system, anharmonicity and electron correlation effects led to an overestimation of the vibrational spectrum calculated.[39] In order to determine the real IR-relation in the complexes, the graphical correlation between experimental and DFT theoretical analysis was plotted as shown in Figs. S4 and S5. It was found that experimental and theoretical IR analyses were excellently matched, resulting in an R^2 value of 0.998 for both complexes. Consequently, the proposed structure of the complexes has been confirmed.

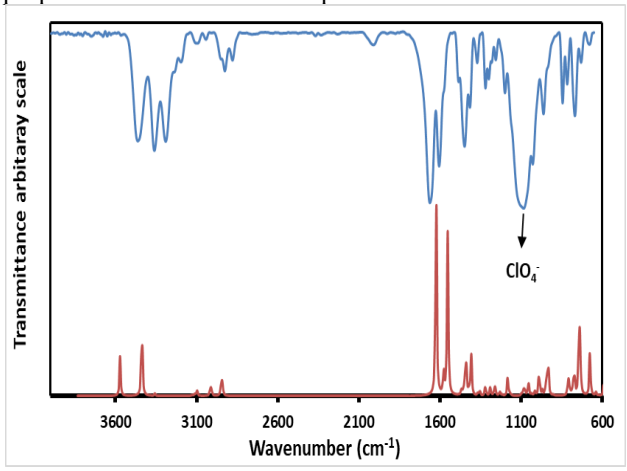

Fig. 4. The experimental FT-IR spectrum of $[NiL_2](ClO_4)_2$ (top), and the calculated IR for $[NiL_2]^{2+}$ at B3LYP/LanLD2Z level of theory (bottom).

Chromotropism

Halochromism study. An aqueous solution of $[NiL_2](ClO_4)_2$ was examined using visible absorption spectroscopy at different pH levels, including the original pH (8.04), alkaline pH (13.000), and acidic pH (1.95). As a result, both the position and intensity of the absorption spectra remained unchanged after 24 hours. There is a visible color change in acidic media, but not in alkaline media. A study of the visible electronic spectra of the solution was conducted over a pH range of 8.04-1.95. Absorbance was not affected by pH below this range. The color of the solution changed significantly from purple to blue after the addition of perchloric acid (0.01 M). In accordance with expectations, the absorption band at 556 nm gradually shifted to 601 nm with decreasing intensity (Fig. 5). There are two isosbestic points at 620 and 739 nm associated with the color change. A spectrophotometric titration of the complex with perchloric acid at 556 nm (inside Fig. 5) demonstrated that two equivalent protons are consumed during the reaction. It seems when the complex was dissolved in water, two water molecules were replaced by the labile amide moiety of the ligand. As a result of their coordination with the metal center, coordinated water molecules become acidic with *pKa* values of 4.5 and 7.5.[40] As illustrated in Scheme 2, a proton transfer occurs from water molecules to amide groups due to the presence of an initial basic medium (initial pH of 8.04) and the acidic nature of the coordinated water molecules. This was supported by a comparison of the visible spectrum of $[NiL_2](ClO_4)_2$ with that of $[Ni(pic)_2(H_2O)_2](ClO_4)_2$ (pic = picolylamine) that its structure is like **1** but without amide arms.[34] Fig. 6 shows that the positions and patterns of the two spectra are almost identical. Therefore, as shown in Scheme 2, in an acidic solution, the isosbestic points may result from the protonation of the coordinated two hydroxo groups located on the axial position of the complex. The suggested mechanism for this observation can be shown in Scheme 2. When complexes are titrated with perchloric acid, two hydroxo groups are protonated, resulting in a blue color. For the purpose of verifying the proposed mechanism, the visible spectrum of $[NiL_2](ClO_4)_2$ was compared with that of acidified $[Ni(pic)_2(H_2O)_2](ClO_4)_2$ (pic = picolylamine). As shown in Fig. 7, the patterns and peak positions in the two spectra are nearly identical. However, by adding NaOH (0.01 M) to the acidified aqueous solution and achieving the initial pH, the original color was restored. In spite of using an additional NaOH and an increase in pH to 13.0, no change in color or visible spectrum of the complex was observed. The visible spectra of complex **1** as a function of pH are shown in Fig. S7. However, spectrophotometric titration at 556 nm with NaOH at pH 12.96 (inside Fig. S7) demonstrated that two equivalents of protons were released from the complex. The observation is consistent with the suggested mechanism. When the complex is titrated with NaOH, the uncoordinated protonated amide moieties are neutralized. As expected, the coordination environment around the nickel center remains unchanged, and neither color nor absorption band changes.

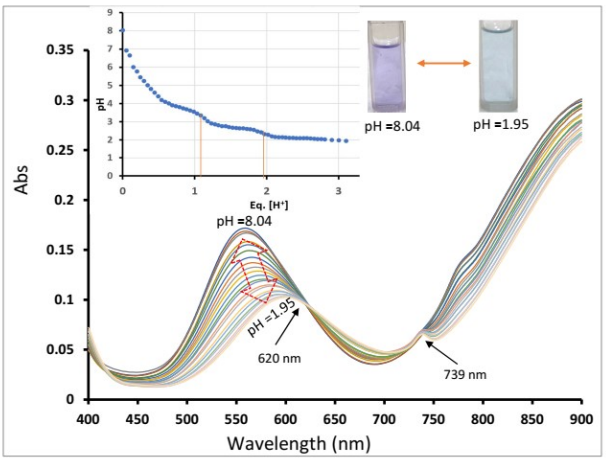

Fig. 5. The spectra of aqueous solution of $[NiL_2](ClO_4)_2$ (0.02 M) in at 25 °C as a function of pH. The inside graph displays the pH (8.04-1.95) against equivalent $[H^+]$ at λ = 560 nm after titration with perchloric acid (4 mM in H_2O).

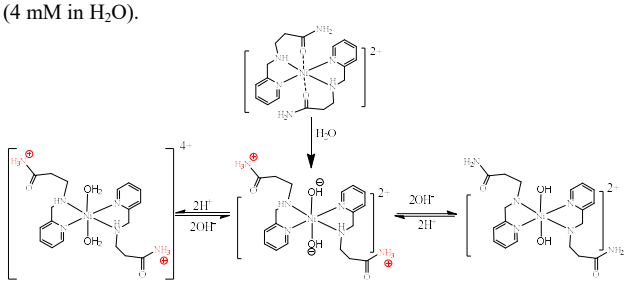

Scheme 2. Interconversion of $[NiL_2]^{2+}$ triggered by acid and base (pH = 1.95-13.00) in aqueous solution

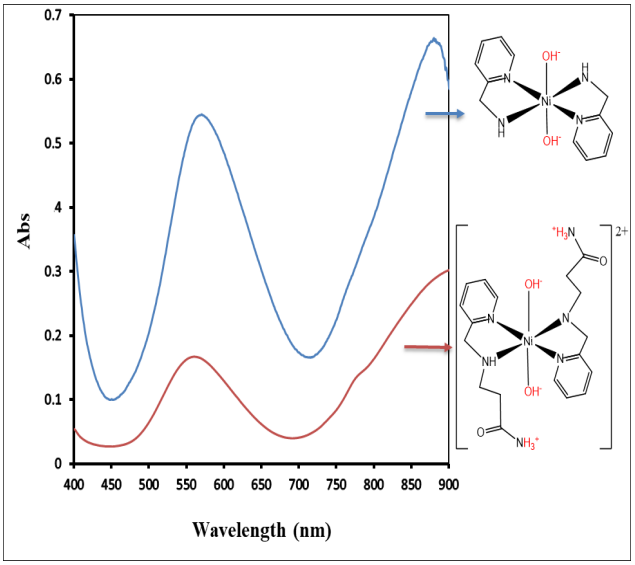

Fig. 6. The visible spectra of $[NiL_2](ClO_4)_2$ (0.02 M) (down) and $[Ni(pic)_2(OH)_2](ClO_4)_2$ (0.02 M) (up) in aqueous solution pH = 8.0.

A similar spectrum can be observed for $[Ni(pic)_2(H_2O)_2](ClO_4)_2$ in an alkaline environment (Fig. 8). The observed small shift can be attributed to the more anionic nature of $[Ni(pic)_2(OH)_2]^{2-}$ compared to the neutral compound $[NiL_2(OH)_2]$. The reversibility of the color and absorbance changes can be reproduced even after five cycles without a decrease in absorbance (Fig. S8).

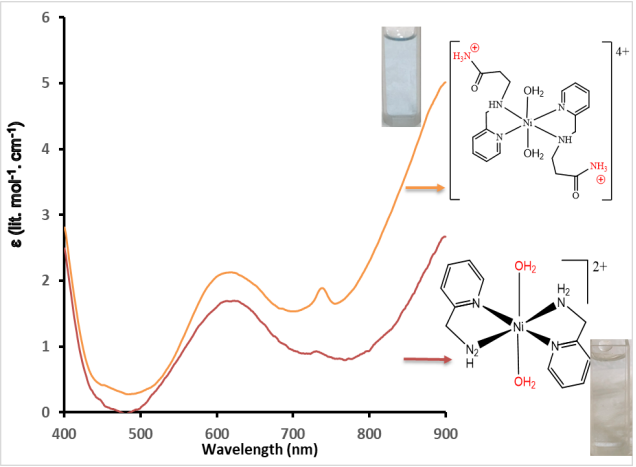

Fig. 7. The visible spectra of $[NiL_2](ClO_4)_2$ (0.02 M) (up) and $[Ni(pic)_2(H_2O)_2](ClO_4)_2$ (0.02 M) (down) in acidic aqueous solution (pH = 2.04).

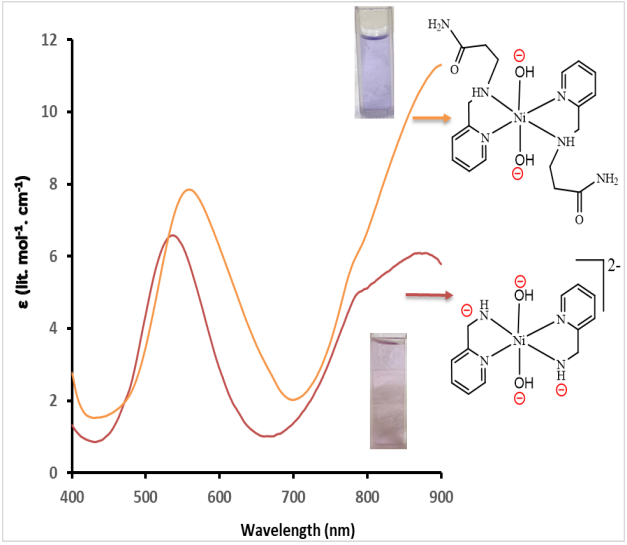

Fig. 8. The visible spectra of $[NiL_2](ClO_4)_2$ (0.02 M) (up) and $[Ni(pic)_2(H_2O)_2](ClO_4)_2$ (0.02 M) (down) in alkaline aqueous solution (pH = 12.51).

Thermochromism study. A thermochromic effect is observed in $[NiL_2](ClO_4)_2$ in solvents with high boiling points. At temperatures ranging from 25 to 180 °C, the visible absorption spectra of 1 in DMSO were measured (Fig. 9). Heating results in the browning of the solution and the appearance of the new band at 462 nm. As the temperature increased, neither the d-d band at 564 nm nor the one above 900 nm changed. Spectra analyzed as a function of temperature reveal no significant differences in color or spectrum up to 110 ºC (Fig. 10). After heating to 150 °C, an isosbestic point was observed at 745 nm and a band at 462 nm formed (Fig. 11). When the temperature was increased to 180º C, two isosbestic points were observed at 648 and 693 nm. Temperature dependence of **1** can be explained by labile amid groups dissociating at high temperatures and being replaced by solvent molecules. The first isosbestic point may be involved in the dissociation of the first amide moiety and the other isosbestic points may be related to the dissociation of the second amide group. In order to confirm this mechanism, $[Ni(pic)_2(H_2O)_2](ClO_4)_2$ was dissolved in DMSO and heated at 180°C that resulted in the development of a new band in the same region as shown in Fig. 12. The process is reversible. Thus, when the solution is cooled, the dangling amide groups re-coordinate with the nickel, regenerating the original color. The same spectrum appears after ten cycles of heating to 180 °C and cooling back to room temperature (Fig S9). A similar phenomenon was observed in the solvent of DMF (Fig. S10).

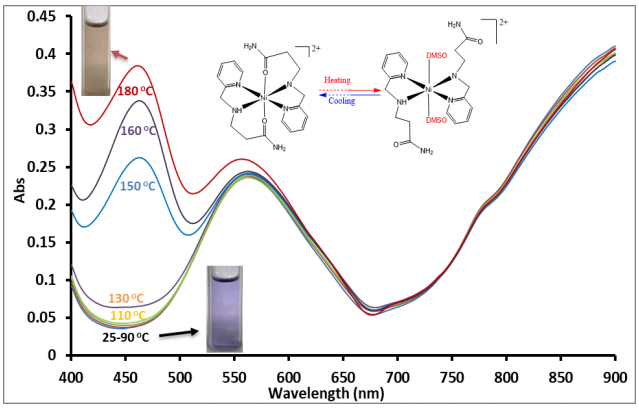

Fig. 9. Temperature dependence of the visible absorbance of DMSO solution of $[NiL_2]$ $(ClO_4)_2$ (0.02 M). Inside figure shows the change in the structure of the complex after heated and cooled in DMSO.

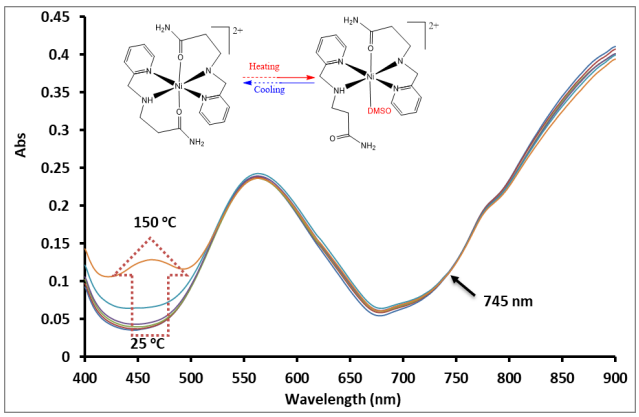

Fig. 10. Temperature dependence of the visible absorbance of DMSO solution of $[NiL_2](ClO_4)_2$ (0.02 M) at temperature interval of 25-150 °C.

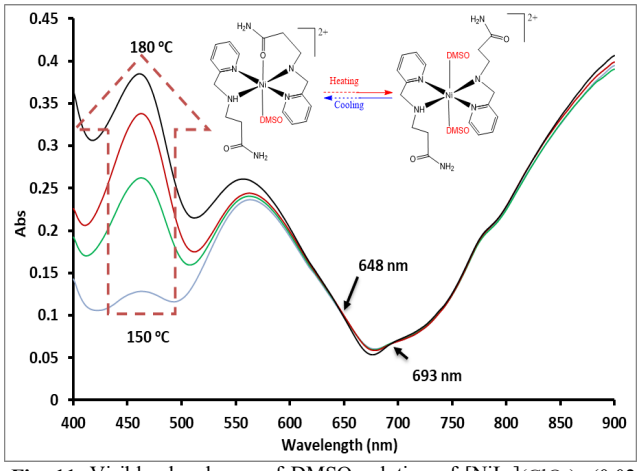

Fig. 11. Visible absorbance of DMSO solution of $[NiL_2](ClO_4)_2$ (0.02 M) as a function of temperature at temperature interval of 150-180 °C.

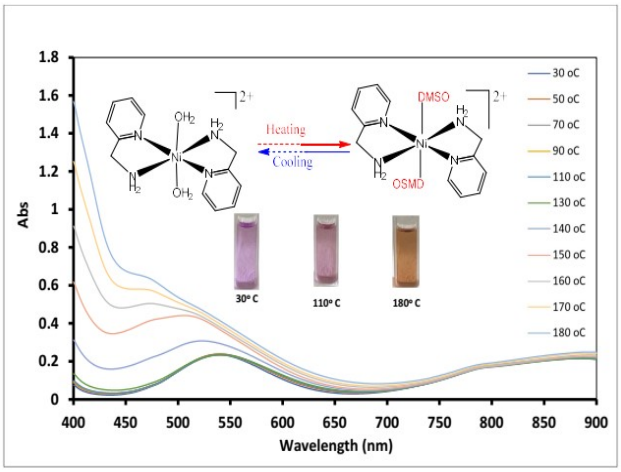

Fig. 12. Temperature dependence of the visible absorbance of DMSO solution of $[Ni(pic)_2(H_2O)_2](ClO_4)_2$ (0.02 M). Inside figure shows the change in the structure of the complex after heated and cooled in DMSO.

4. CONCLUSION

In the current research, Ni(II) and Zn(II) complexes of the N-(2-propanamide)-2-picolylamine ligand were prepared and characterized. The geometric structures of the complexes are octahedral and ligand in both complexes acts as tridentate NNO donors. Additionally, the structures of the compounds, their bond lengths, and their bond angles were determined by the Gaussian 09 program at the B3LYP/LanL2DZ level. Visible spectroscopy was also used to examine Ni(II) complex halochromism and thermochromism. Halochromism occurs when labile moieties of the ligand undergo protonation and deprotonation, resulting in a distinct color change from purple to blue. It was observed that the complex exhibited reversible thermochromism in solvents containing DMSO or DMF as a result of the dissociation of hemilabile amide moieties from the metal center and their substitution by solvent molecules.

CONFLICTS OF INTEREST

ACKNOWLEDGMENTS

We are grateful for the financial support of University of Mazandaran of the Islamic Republic of Iran.

AUTHOR INFORMATION

Corresponding Authors

Hamid Golchoubian, Email: h.golchobian@umz.ac.ir, *ORCID: 0000-0001-9794-4187*

Atie Shirvan: Email: at.shirvan@gmail.com, *ORCID: 0000-0002-2324-5743*

Author

Marzieh Asadollahi

REFERENCES

1. P. Braunstein, F. Naud, *Angew. Chem. Int. Ed.* **2001**, *40*, 680-699.
2. G. M. Adams, A. S. Weller, *Coord. Chem. Rev.* **2018**, *355*, 150-172.
3. C. S. Slone, D. A. Weinberger, C. A. Mirkin, *Prog. Inorg. Chem.* **1999**, *48*, 233-350.
4. A. Bader, E. Lindner, *Coord. Chem. Rev*. **1991**, *108*, 27-110.
5. E. Lindner, S. Pautz, M. Haustein, *Coord. Chem. Rev*. **1996**, *155*, 145-162.
6. K. D. Hesp, D. Wechsler, J. Cipot, A. Myers, R. McDonald, M. J. Ferguson, G. Schatte, M. Stradiotto, *Organometal*. **2007**, *26*, 5430-3437.
7. J. Duran, D. Oliver, A. Polo, J. Real, J. Benet-Buchholz, X. Fontrodona, *Tetrahedron: Asymmetry* **2003**, *14,* 2529-2538.
8. Y. S. Uh, A. Boyd, V. R. Little, P. G. Jessop, K. D. Hesp, J. Cipot-Wechsler, M. Stradiotto, R. McDonald, *J. Organomet. Chem*. **2010**, *695*, 1869-1872.
9. M. J. Wiester, C. A. Mirkin, *Inorg. Chem*. **2009**, *48*, 8054-8056.
10. E. Lindner, I. Warad, K. Eichele, H. A. Mayer *Inorg. Chim. Acta* **2003**, *350*, 49-56.
11. S. E. Angell, C. W. Rogers, Y. Zhang, M. O. Wolf, Jr. W. E. Jones, *Coord. Chem. Rev*. **2006**, *250*, 1829-1841.
12. L. Rostami, H. Golchoubian, *J. Coord. Chem*. **2017**, *70*, 3660-3676.
13. M. Ghoreishi Amiri, H. Golchoubian, *J. Mol. Struct*. **2018**, *1165*, 196-205.
14. H. Golchoubian, A. Heidarian, E. Rezaee, F. Nicolò, *Days & Pigments* **2014**, *104,* 175-184.
15. Y. Fukuda, Inorganic Chromotropism: Basic Concepts and Applications of Colored Materials, Springer, Germany, **2007**.
16. U. El-Ayaan, F. Murata, Y. Fukuda, *Monatshe. Chem*. **2001**, *132*, 1279-1294.

17. H. Golchoubian, S. Nateghi, *J. Coord. Chem*. **2016**, *69*, 3192-3205.
18. A. Shirvan, H. Golchoubian, E. Bouwman, *J. Mol. Struct*. **2019**, *1195*, 769-777.
19. M. J. Frisch, G. W. Trucks, H. B. Schlegel, G. E. Scuseria, M. A. Robb, J. R. Cheeseman, G. Scalmani, V. Barone, B. Mennucci, G. A. Petersson, H. Nakatsuji, M. Caricato, X. Li, H. P. Hratchian, A. F. Izmaylov, J. Bloino, G. Zheng, J. L. Sonnenberg, M. Hada, M. Ehara, K. Toyota, R. Fukuda, J. Hasegawa, M. Ishida, T. Nakajima, Y. Honda, O. Kitao, H. Nakai, T. Vreven, J. A. Montgomery Jr., J. E. Peralta, F. Ogliaro, M. Bearpark, J. J. Heyd, E. Brothers, K. N. Kudin, V. N. Staroverov, R. Kobayashi, J. Normand, K. Raghavachari, A. Rendell, J. C. Burant, S. S. Iyengar, J. Tomasi, M. Cossi, N. Rega, J. M. Millam, M. Klene, J. E. Knox, J. B. Cross, V. Bakken, C. Adamo, J. Jaramillo, R. Gomperts, R. E. Stratmann, O. Yazyev, A. J. Austin, R. Cammi, C. Pomelli, J. W. Ochterski, R. L. Martin, K. Morokuma, V. G. Zakrzewski, G. A. Voth, P. Salvador, J. J. Dannenberg, S. Dapprich, A. D. Daniels, O. Farkas, J. B. Foresman, J. V. Ortiz, J. Cioslowski, D. J. Fox, Gaussian 09. Revision A. 1, Gaussian Inc., Wallingford, USA **2009**.
20. R. Dennington, T. Keith, J. Millam, GaussView, Version 5, Semichem Inc., Shawnee Mission, **2009**.
21. B. P. Pritchard, D. Altarawy, B. Didier, T. D. Gibson, T. L. Windus, *J. Chem. Info. Model,* **2019**, *59*, 4814-4820.
22. W. -Y. Wang, X. -F. Du, N. -N. Ma, S. -L. Sun, Y. -Q. Qiu, *J. Mol. Model*. **2013**, *19*, 1779-1787.
23. B. Machura, J. G. Małecki, A. S. Witlicka, I. Nawrot, R. Kruszynski, *Polyhedron* **2011**, *30*, 864-872.
24. F. Billes, A. Holmgren, H. Mikosch, *Vib. Spectrosc*. **2010**, *53*, 296-306.
25. Z. Demircioglu, C. A. Kastas, O. Buyukgungor, *Spectrochim. Acta A* **2015**, *139*, 539-548.
26. J. Fleming, Frontier Orbitals and Organic Chemical Reactions, Wiley, London, **1976**.
27. K. Fukui, *Science* **1982**, *218*, 747-754.
28. C. J. Brabec, N. S. Sariciftci, J. C. Hummelen, *Adv. Funct. Mater*. **2001**, *11*, 374-380.
29. E. E. Ebenso, T. Arslan, F. Kandemirli, I. Love, C. Ogretir, M. Saracoglu, S. A. Moron, *Int. J. Quantum. Chem*. **2010**, *110*, 2614-2636.
30. H. Golchoubian, E. Rezaee, *J. Mol. Struct.* **2009**, *927*, 91-95.
31. Y. Fukuda, A. Shimura, M. Mukaida, E. Fujita, K. Sone, *J. Inorg. Nucl. Chem*. ***1974****, 36, 1265-1270.*
32. W. J. Geary, *Coord. Chem. Rev*., **1971**, *7*, 81-122.
33. J. R. Hartman, R. W. Vachet, J. H. Callahan, *Inorg. Chim. Acta* **2000**, *297*, 79-87.
34. S. Kazemi, H. Golchoubian, *Inorg. Chem. Res*., **2020**, *4*, 76-85.
35. A. B. P. Lever, Inorganic Electronic Spectroscopy, 2nd edn., Elsevier, Amsterdam, **1984**.
36. G. Bruhn, E. R. Davidson, I. Mayer, A. E. Clark, *Chem. Rev*. **2006**, *106*, 2065-2072.
37. E. Ebenso, M. M. Kabanda, T. Arslan, M. Saracoglu, F. Kandemirli, L. C. Murulana, A. K. Singh, S. K. Shukla, B. Hammouti, K. F. Khaled, M. A. Quraishi, I. B. Obot, N. O. Edd, *Int. J. Electrochem. Sci*. **2012**, *7*, 5643-5676.
38. I. Sheikhshoaie, S. Y. Ebrahimipour, A. Crochet, K. Fromm, Synthesis, *Res. Chem. Intermed*. **2015**, *41*, 1881-1891.
39. A. Atac, C. Karaca, S. Gunnaz, M. Karabacak, *Spectrochim. Acta A* **2014**, *130*, 516-525.
40. R. G. Wilkines, Kinetics and mechanism of reaction of transition metal complexes 2nd Ed. Wiely-VCH Verlag GmbH & Co KGaA, Weinheim, **2002**.